Sub-optimal control based wall models for LES — including transpiration velocity

By J. S. Baggett \dagger , F. Nicoud \ddagger , B. Mohammadi \P , T. Bewley \parallel J. Gullbrand $\dagger\dagger$, and O. Bottela $\ddagger\ddagger$

1. Introduction

1.1. Background

One of the primary reasons that Large Eddy Simulation (LES) is not yet practical for many flows of engineering interest is the high resolution required in turbulent boundary layers. The only way to simulate many flows is to completely bypass the simulation of the near-wall turbulence and to model its effects on the flow away from the wall. If the near-wall flow is not computed then the no-slip boundary condition does not apply and the wall stresses are required to close the usual finite difference approximations to the viscous terms.

The simplest wall stress models correlate the wall stresses to the tangential velocities at the first off-wall grid points. More complex models for the wall stresses rely on the integration of boundary layer equations on an auxiliary mesh embedded near the wall. See Cabot & Moin (2000) for a recent review of wall stress models. These models perform adequately at low to moderate Reynolds numbers in simple flows, but they fail to produce good results at higher Reynolds numbers even in simple channel flow (Nicoud et al. (2000)). The current generation of wall stress models attempts to reproduce the physics of the wall stresses averaged over the filter width of the outer LES computation. However, none of these models can compensate for the numerical and subgrid-scale (SGS) modeling errors that are intrinsic to an LES computation which necessarily relies on a low-order numerical scheme and an exceedingly coarse near-wall mesh.

To find wall models, in the form of approximate boundary conditions, that can compensate for the errors intrinsic to under-resolved LES, we use techniques from optimal control theory. In our approach, a sub-optimal control strategy is used in which the objective is to force the outer LES towards a desired solution by using the approximate boundary conditions as control. In previous work (Nicoud et al. (2000)), this approach was tested by using wall stress boundary conditions as control to force the mean velocity of a coarse-grid LES of channel flow at high Reynolds number towards a logarithmic velocity profile. It was found that the resulting wall stress boundary conditions yielded much better results, in terms of the mean velocity profile, than existing wall stress models at high Reynolds numbers. Furthermore, it was found that the resulting wall stresses were well correlated with the local velocity field and that the dynamically relevant portion of the wall stresses could be predicted by a relatively simple linear model.

```
† University of Wisconsin – La Crosse, WI, USA
‡ CERFACS, France
¶ University of Montpellier and INRIA, France
∥ Univ. Calif. San Diego, CA, USA
†† CTR
‡‡ CTR
```

Furthermore, it was found that the wall stresses generated by the sub-optimal control strategy, while improving the prediction of the mean velocity profile considerably, did not improve the prediction of the velocity fluctuations. This may have been due to the inadequacy of the dynamic Smagorinsky sub-grid scale model in the anisotropic logarithmic region of the channel flow, but it could also have been that wall stress boundary conditions alone cannot fully compensate for the errors in the vicinity of the computational boundary. Generally, any improvements in the prediction of the outer flow were limited primarily to a region extending only a few grid cells from the wall.

When wall stress boundary conditions are used to model the influence of the near-wall region on the outer flow, it is usually assumed that the wall-normal velocity is identically zero at the boundary. However, since the no-slip boundary condition cannot be applied without adequate near-wall resolution, perhaps it does not make sense to insist that the velocity normal to the boundary is zero. After all, a wall model should capture the effects of the near-wall turbulence on the outer flow, including such hallmarks of near-wall turbulence as ejections and sweeps. In any case, the combination of non-zero boundary-normal velocity with wall stresses should allow the approximate boundary condition wall model to influence more of the computational domain than wall stress boundary conditions alone since the boundary-normal velocity effects the entire flow directly via the continuity equation.

It is the objective of the current work to test the effect of including a transpiration velocity approximate boundary condition (net transpiration will be zero) in addition to the wall stress boundary conditions in the sub-optimal control framework first explored in Nicoud et al. (2000). The sub-optimal control framework, including transpiration velocity, was first presented in Nicoud & Baggett (1999), but it is presented again here in a slightly more general form. We also discuss whether or not simple, algebraic models derived from the sub-optimally controlled simulations are likely to be successful.

2. Sub-optimal control framework

2.1. Channel flow

We consider the LES of incompressible, turbulent channel flow on a uniform mesh with 32 volumes in the streamwise and spanwise directions and 33 volumes in the wall-normal direction. A staggered grid system is used with second order finite differences for the spatial derivatives and a third-order Runga-Kutta discretization for the time advancement. Periodic boundary conditions are imposed in the two directions x_1 and x_3 (or x and z) parallel to the walls. The SGS model is the Smagorinsky model with the coefficient determined by the plane-averaged dynamic procedure of Germano $et\ al.\ (1991)$. Unless otherwise stated, all quantities are nondimensionalized by the friction velocity, u_{τ} , and channel half-height, h. The channel walls are at $y=\pm 1$. The skin friction Reynolds number is defined as $\text{Re}_{\tau}=u_{\tau}h/\nu$. When the mean flow is statistically converged the mean streamwise pressure gradient is equal to the wall stress, that is, $-\partial P/\partial x = \langle \tau_w \rangle = 1$. All of the simulations in this work were performed at $\text{Re}_{\tau}=4000$ in a computational domain with dimensions $2\pi h \times 2h \times 2\pi h/3$ in the streamwise $(x_1\ \text{or}\ x)$, wall-normal $(x_2\ \text{or}\ y)$, and spanwise $(x_3\ \text{or}\ z)$ directions, respectively.

The governing equations are:

$$\frac{\partial u_i}{\partial t} + \frac{\partial u_i u_j}{\partial x_i} = -\frac{\partial P}{\partial x_i} + \frac{\partial}{\partial x_j} \left((\nu + \nu_t) \left(\frac{\partial u_i}{\partial x_j} + \frac{\partial u_j}{\partial x_i} \right) \right)$$

(2.1)

$$\frac{\partial u_j}{\partial x_i} = 0$$

The pressure, P, contains a mean forcing component such that $\langle -\partial P/\partial x \rangle = 1$. Note that no specific notation is used to describe spatial filtering associated with the LES formulation, rather each variable, herein, should be understood as the filtered counterpart of the actual variable (e.g. $u_i \equiv \bar{u_i}$).

Since the no-slip boundary condition does not apply on the coarse mesh used here, the boundary conditions that are supplied are the wall stresses τ_{12}^w and τ_{32}^w as well as the normal velocity at the wall, v_w . The boundary conditions, specified in terms of the control parameter, phi, which is defined below, on (2.1) are:

$$\frac{\partial u}{\partial y_n} + \frac{\partial v_n}{\partial x} = \frac{1}{\nu_w} \phi_u$$

$$v_n = \phi_v$$

$$\frac{\partial w}{\partial y_n} + \frac{\partial v_n}{\partial z} = \frac{1}{\nu_w} \phi_w$$
(2.2)

where the subscript n stands for the outward normal to the wall and ν_w is the wall value of the total dynamic viscosity $\nu + \nu_t$ (in this work $\nu_w \equiv \nu$). The control parameter ϕ is defined as $\phi = (\phi_u, \phi_v, \phi_w) = (\tau_{12}^w, v_w, \tau_{32}^w)$ at y = +1 and $\phi = (\phi_u, \phi_v, \phi_w) = -(\tau_{12}^w, v_w, \tau_{32}^w)$ at y = -1.

2.2. Objective function

In the sub-optimal control approach, the boundary conditions (specified by the control parameter ϕ) are used as control to minimize an objective function at each time step. The goal being to provide numerical boundary conditions to the flow solver so that the overall solution is consistent with what is expected in a channel flow. The objective function is specified as follows:

$$\mathcal{J}(u;\phi) = \sum_{i=1,3} \mathcal{J}_{\text{mean},i}(u;\phi) + \sum_{i=1}^{3} \mathcal{J}_{\text{rms},i}(u;\phi) + \sum_{i=1}^{3} \mathcal{J}_{\text{penalty},i}(\phi).$$
 (2.3)

The objective function consists of the three components. \mathcal{J}_{mean} measures the distance from the plane-averaged LES solution to a desired reference velocity profile. The second component, \mathcal{J}_{rms} measures the distance from the plane-averaged velocity fluctuation intensities to desired target profiles. Finally, the third component, $\mathcal{J}_{penalty}$ penalizes the use of large controls ϕ . The component objective functions are defined below.

For the mean streamwise velocity the target or reference profile is taken as a logarithmic velocity profile throughout the channel: $u_{1,\mathrm{ref}}^+ = \kappa^{-1} \ln y^+ + C$. The spanwise velocity reference profile is simply $u_{3,\mathrm{ref}} \equiv 0$. The difference between the reference velocity profile and the plane-averaged LES solution is a function of the wall-normal coordinate, y, and can be expressed as

$$\delta_{u_i}(y) = \frac{1}{A} \int \int (u_i - u_{i,ref}) \, dx \, dz \qquad (i = 1, 3)$$
 (2.4)

where A is the channel area in the homogeneous plane. Note that any reference profile suitable for a parallel flow could have been used. Notably, a more realistic shape could have been used near the channel center. However, the logarithmic profile is well suited

for the near-wall region since we are using a coarse mesh and the Reynolds number, $\text{Re}_{\tau} = 4000$, is sufficiently high so that the first grid point lies in the logarithmic region $(y^+ \approx 121)$. The mean component of the objective function is then:

$$\mathcal{J}_{\text{mean},i}(u;\phi) = \alpha_i \int_{-1}^{+1} \delta_{u_i}(y)^2 \, dy, \qquad (i=1,3)$$
 (2.5)

Note that there is no need to specify a target profile for the plane-averaged wall-normal velocity since that will be identically zero at each time step provided there is no net transpiration velocity through the boundaries.

The velocity fluctuation intensities are targeted through the \mathcal{J}_{rms} component of the objective function. The plane-averaged, mean square velocity fluctuations are compared at each time step to the mean square velocity fluctuations, $(u'_{i,ref})^2$, from the LES of Kravchenko, Moin & Moser (1996) which was performed at the same Reynolds number, $Re_{\tau} = 4000$, using a zonally defined mesh to resolve the near-wall region. The distance between the plane-averaged mean square velocity fluctuations and their reference profiles can be measured as

$$\delta_{u_i'}(y) = \frac{1}{A} \int \int \left((u_i - \langle u_i \rangle)^2 - u_{i,\text{ref}}'^2 \right) dx dz, \qquad (i = 1, 2, 3), \tag{2.6}$$

where $\langle u_i \rangle$ denotes the average over the homogeneous directions of the velocity component u_i . The velocity fluctuation intensity component of the objective function is then

$$\mathcal{J}_{\text{rms},i}(u;\phi) = \beta_i \int_{-1}^{+1} \delta_{u_i'}(y)^2 \, dy \qquad (i=1,2,3)$$
 (2.7)

Finally, to prevent numerical instabilities it is necessary to regularize the control, that is, the approximate boundary conditions, by including a penalty component in the overall objective function:

$$\mathcal{J}_{\text{penalty},i}(\phi) = \frac{\gamma_i}{A} \int_{y=\pm 1} \phi_{u_i}^2 \, dx \, dz + \frac{\lambda}{A} \int_{y=\pm 1} \delta_{i2} \phi_{u_2}^4 \, dx \, dz \qquad (i = 1, 2, 3). \tag{2.8}$$

The first term in the penalty component attempts to prevent the mean square norm of the control parameter from becoming too large. In the case of transpiration velocity control, however, it was found that it is necessary to prevent the transpiration velocity from becoming too large at any single point, hence the second term in the penalty component (2.8) was added.

Note that each component of the objective function includes a scalar parameter: α_i , β_i , γ_i , or λ . These scalars allow the relative importance of the various objectives to be changed in the overall objective.

2.3. Adjoint problem

The gradient of the objective function \mathcal{J} with respect to the control parameter ϕ is estimated by using the Fréchet differential (Vainberg (1964)) defined for any functional F as:

$$\frac{DF}{D\phi}\tilde{\phi} = \lim_{\epsilon \to 0} \frac{F(\phi + \epsilon\tilde{\phi}) - F(\tilde{\phi})}{\epsilon},\tag{2.9}$$

where $\tilde{\phi}$ is an arbitrary direction. From (2.3) the gradient \mathcal{J} is:

$$\frac{D\mathcal{J}}{D\phi}\tilde{\phi} = \sum_{i=1,3} \alpha_i \int \int \int_{\Omega} 2\frac{\delta_{u_i}}{A} \mathcal{U}_i \, dx \, dy \, dz$$

Sub-optimal control based wall models for LES

$$+\sum_{i=1}^{3} \beta_{i} \int \int \int_{\Omega} 2 \frac{\delta_{u'_{i}}(u_{i} - \langle u_{i} \rangle)}{A} \mathcal{U}_{i} dx dy dz$$

$$+\lambda \frac{4}{A} \int \int_{u=+1} \phi_{u_{2}}^{3} \tilde{\phi}_{u_{2}} dx dz + \sum_{i=1}^{3} \gamma_{i} \frac{2}{A} \int \int_{u=+1} \phi_{u_{i}} \tilde{\phi}_{u_{i}} dx dz$$

$$(2.10)$$

5

where \mathcal{U}_i denotes the Fréchet derivative of $u_i\dagger$. The gradient of \mathcal{J} cannot be calculated directly from (2.10) since the derivatives \mathcal{U}_i are unknown.

To calculate an approximation to the gradient of \mathcal{J} we start by assuming that the equation of state, (2.1), is discretized in time by a semi-implicit discretization:

$$u_i^{n+1} + \Delta t \left[\frac{\partial P}{\partial x_i} + \frac{\partial u_i u_j}{\partial x_j} - \frac{\partial}{\partial x_j} \left((\nu + \nu_t) \left(\frac{\partial u_i}{\partial x_j} + \frac{\partial u_j}{\partial x_i} \right) \right) \right]^{n+1} = \text{RHS}^n$$

$$-\Delta t \frac{\partial u_j^{n+1}}{\partial x_i} = 0$$
(2.11)

with the boundary conditions (2.2). The terms which depend only on the variables at the previous time step n are gathered in the generic notation RHSⁿ and disappear in the analytical development.

We now formulate an adjoint problem to find the gradient (2.10). The first step is to take the derivative of (2.11) with respect to the control ϕ :

$$\mathcal{U}_{i} + \Delta t \left[\frac{\partial \mathcal{P}}{\partial x_{i}} + \mathcal{U}_{j} \frac{\partial u_{i}}{\partial x_{j}} + u_{j} \frac{\partial \mathcal{U}_{i}}{\partial x_{j}} - \frac{\partial}{\partial x_{j}} \left((\nu + \nu_{t}) \left(\frac{\partial \mathcal{U}_{i}}{\partial x_{j}} + \frac{\partial \mathcal{U}_{j}}{\partial x_{i}} \right) \right) \right] = 0$$

$$-\Delta t \frac{\partial \mathcal{U}_{j}}{\partial x_{j}} = 0$$

$$(2.12)$$

with boundary conditions:

$$\frac{\partial \mathcal{U}}{\partial y_n} + \frac{\partial \mathcal{V}_n}{\partial x} = \frac{1}{\nu_w} \tilde{\phi}_u$$

$$\mathcal{V}_n = \tilde{\phi}_v$$

$$\frac{\partial \mathcal{W}}{\partial y_n} + \frac{\partial \mathcal{V}_n}{\partial z} = \frac{1}{\nu_w} \tilde{\phi}_w.$$
(2.13)

The righthand side term in (2.12) is now zero since the flow field at time step n does not depend on the control ϕ for the current time step. Therefore, the superscript n+1 has been dropped for clarity. Note also in (2.12) that the Fréchet derivative of the eddy viscosity was assumed to be zero, that is, $D\nu_t/D\phi = 0$. The latter approximation can be justified for short time intervals; see Collis & Chang (1999). Moreover, this system of equations is linear in the variables \mathcal{U}_i and \mathcal{P} , where \mathcal{P} is the Fréchet derivative of the pressure. Therefore it can be written in the form:

$$\mathcal{A}\Theta = 0, \tag{2.14}$$

† Technically, the second term in (2.10) should include the integral $\int \int \int_{\Omega} 2 \frac{\delta_{u_i'}(u_i - \langle u_i \rangle)}{A} (\mathcal{U}_i - \langle \mathcal{U}_i \rangle) \, dx \, dy \, dz, \text{ but we make the approximation that } \langle \mathcal{U}_i \rangle \equiv 0 \text{ since } |\langle \mathcal{U}_i \rangle| \ll |\mathcal{U}_i| \text{ in general.}$

where \mathcal{A} is the linear operator acting on the vector $\Theta = (\mathcal{U}_i, \mathcal{P})^T$. The linear system (2.14) with unknown boundary conditions (2.13) cannot be solved directly, instead, an adjoint operator, \mathcal{A}^* , is formulated by considering the equation

$$\langle \mathcal{A}\Theta, \Psi \rangle = \langle \Theta, \mathcal{A}^*\Psi \rangle + BT,$$
 (2.15)

where $\langle \cdot, \cdot \rangle$ stands for the inner product defined as the integral over the flow domain of the dot product of the two vectors and Ψ is the adjoint state vector $\Psi = (\eta_i, \pi)^T$. Finding the adjoint operator, \mathcal{A}^* , and the boundary terms, BT, is a straightforward exercise in integrating by parts. The adjoint operator acting on the adjoint state vector, that is, $\mathcal{A}^*\Psi$ is defined by the equations:

$$\mathcal{A}^* \Psi = \begin{cases} \eta_i + \Delta t \left[\frac{\partial \pi}{\partial x_i} + \eta_j \frac{\partial u_j}{\partial x_i} - u_j \frac{\partial \eta_i}{\partial x_j} - \frac{\partial}{\partial x_j} \left[(\nu + \nu_t) \left(\frac{\partial \eta_i}{\partial x_j} + \frac{\partial \eta_j}{\partial x_i} \right) \right) \right] \\ -\Delta t \frac{\partial \eta_j}{\partial x_j} \end{cases}$$
(2.16)

and the boundary terms are:

$$BT = \Delta t \int \int_{y=\pm 1} (Press + Conv + Visc) \, dx \, dz$$
 (2.17)

with

Press =
$$\mathcal{P}\eta_{2n} - \mathcal{V}_n \pi$$

Conv = $\eta_i \mathcal{U}_i v_n$ (2.18)
Visc = $-\nu_w \left[\eta_i \left(\frac{\partial \mathcal{U}_i}{\partial y_n} + \frac{\partial \mathcal{V}_n}{\partial x_i} \right) - \mathcal{U}_i \left(\frac{\partial \eta_i}{\partial y_n} + \frac{\partial \eta_{2n}}{\partial x_i} \right) \right]$.

¿From (2.14), the relation (2.15) defining the adjoint operator reduces to

$$\langle \mathcal{A}^* \Psi, \Theta \rangle = -BT. \tag{2.19}$$

2.4. Gradient estimate

We now have the liberty to choose boundary conditions and right-hand side terms for the adjoint problem such that the relation (2.19) can be utilized to calculate the gradient of \mathcal{J} . By comparing equations (2.10), (2.17), (2.18) and (2.19), it appears that a judicious choice for the definition of the adjoint problem is:

$$\mathcal{A}^* \Psi = \frac{2}{A} \begin{pmatrix} \alpha_1 \delta_u + \beta_1 \delta_{u'} (u - \langle u \rangle) \\ \beta_2 \delta_{v'} (v - \langle v \rangle) \\ \alpha_3 \delta_w + \beta_3 \delta_{w'} (w - \langle w \rangle) \\ 0 \end{pmatrix}$$
(2.20)

with boundary conditions at the wall:

$$\eta_1 v_n + \nu_w \frac{\partial \eta_1}{\partial y_n} = 0$$

$$\eta_{2n} = 0$$

$$\eta_3 v_n + \nu_w \frac{\partial \eta_3}{\partial y_n} = 0.$$
(2.21)

In doing so, (2.19) can be re-written as:

$$\frac{D\mathcal{J}}{D\phi}\tilde{\phi} = -\Delta t \int \int_{y=\pm 1} \left[\eta_1 \tilde{\phi}_u + \left(\pi - 2\nu_w \frac{\partial \eta_{2n}}{\partial y_n} \right) \tilde{\phi}_v + \eta_3 \tilde{\phi}_w \right] dx dz$$

$$+\lambda \frac{4}{A} \int \int_{y=\pm 1} \phi_{u_2}^3 \tilde{\phi}_{u_2} \, dx \, dz + \sum_{i=1}^3 \gamma_i \frac{2}{A} \int \int_{y=\pm 1} \phi_{u_i} \tilde{\phi}_{u_i} \, dx \, dz$$

Since (2.22) is valid for all directions $\tilde{\phi}$, the gradient of \mathcal{J} may be extracted:

$$\frac{D\mathcal{J}}{D\phi_1} = \Delta t \eta_{1,w} + \frac{2\gamma_1}{A} \phi_1
\frac{D\mathcal{J}}{D\phi_2} = \Delta t \left(\pi_w - 2\nu_w \frac{\partial \eta_{2n}}{\partial y_n} \right) + \frac{2\gamma_2}{A} \phi_2 + \frac{4\lambda}{A} \phi_2^3
\frac{D\mathcal{J}}{D\phi_3} = \Delta t \eta_{3,w} + \frac{2\gamma_3}{A} \phi_3,$$
(2.22)

where the subscript w stands for the values at the wall. A control procedure using a simple steepest descent algorithm at each time step may now be proposed such that:

$$\phi^{n+1,k+1} = \phi^{n+1,k} - \mu \frac{D\mathcal{J}(\phi^{n+1,k})}{D\phi}$$
 (2.23)

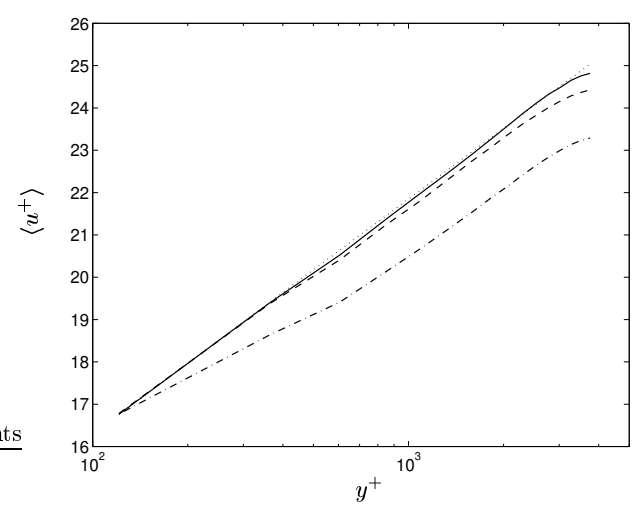
where the parameter μ can be varied to change the rate of convergence and the extra superscript k refers to the subiterations in the descent algorithm. Note that the adjoint operator depends on the state vector $(u_i, P)^T$ at time n+1 so that the state equation and the adjoint problem must be solved simultaneously to obtain the sub-optimal approximate boundary conditions. The adjoint problem (2.20) with boundary conditions (2.21) is discretized and solved using the same numerics as the flow solver. Note that the resulting gradient of the objective function is an approximation since the spatial terms in (2.11) are assumed to be continuous, the gradient of the eddy viscosity, $D\nu_t/D\phi$, is assumed to be zero, and we have omitted a term in (2.10). An exact adjoint problem could be formulated from the fully discretized equations of state, but this is considerably more difficult than the current approach. More details about the algorithm used to solve the adjoint problem may be found in Nicoud $et\ al.\ (2000)$.

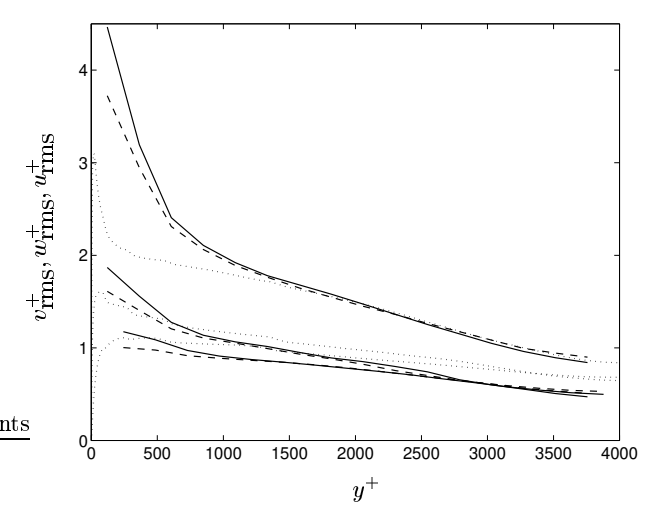
3. Results

3.1. Objective function for mean flow only

The first test is to see if the addition of the transpiration velocity control to the wall stress controls results in an improvement of the prediction of the mean velocity profile. In the following, the reference mean velocity profile is taken as $u_{\text{ref}}^+ = 2.41 \ln y^+ + 5.2$. This version of the logarithmic law was suggested by P. Bradshaw (private communication) for high Reynolds number flows. To test the influence of transpiration velocity only on the mean velocity profile, the constants β_i in the objective function, (2.3), are set to zero so that only the desired mean velocity profile is targeted. For this simulation the parameters in the objective function (2.3) were: $\alpha_1 = \alpha_3 = 1, \beta_1 = \beta_2 = \beta_3 = 0, \gamma_1 = \gamma_3 = 10^{-4}, \gamma_2 = 0.02$, and $\lambda = 0$. The relaxation parameter in the steepest descent algorithm was $\mu = 10^3$.

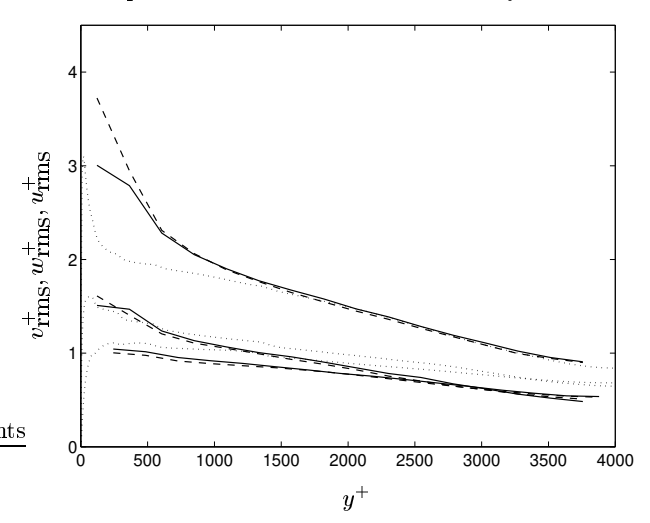
Figure 1 shows that, indeed, the addition of the transpiration control improves the mean velocity profile slightly over the case when only wall stress controls are considered. Also shown in Figure 1 is the mean velocity profile obtained by using the simple wall stress model of Piomelli *et al.* (1989) that correlates the the streamwise wall stress to the streamwise velocity at a point away from the wall and slightly downstream. The





latter model yields results that are typical of most current wall stress models for this flow configuration.

The improvement in the mean velocity profile is encouraging. However, Figure 2 shows the root mean square (rms) velocity fluctuations for the sub-optimal wall stress boundary conditions with and without the addition of transpiration velocity control. The rms velocity fluctuations actually increase with the addition of transpiration which is certainly in the wrong direction since the fluctuation intensities are already over-predicted.



3.2. Objective function including mean flow and rms velocities

In Nicoud *et al.* (2000), it was shown that sub-optimal wall stress boundary conditions alone had little effect on the velocity fluctuation intensities even when the objective function included a component that targeted the fluctuations. The addition of a transpiration velocity control improves matters to some extent. For this simulation the parameters in the objective function (2.3) were: $\alpha_1 = \alpha_3 = 1, \beta_1 = \beta_2 = \beta_3 = 3 \times 10^{-4}, \gamma_1 = 5 \times 10^{-5}, \gamma_2 = 10^{-3}, \gamma_3 = 4 \times 10^{-6}$ and $\lambda = 5 \times 10^{-3}$. The relaxation parameter in the steepest descent algorithm was $\mu = 500$ for ϕ_{u_2} and 10^5 for ϕ_{u_1} and ϕ_{u_3} .

Figure 3 shows the rms velocities when the rms component is included in the objective function. As illustrated in Figure 3, the prediction of the rms velocities improves when the transpiration velocity control is added, however the streamwise rms velocity is still overpredicted near the wall. Not shown for this simulation is the mean velocity profile, which in this case, is not as good as the mean velocity profile that is achieved in the previous section when only the mean velocity profile is targeted by the controls. If shown, it would lie between the two mean velocity profiles in Figure 1 corresponding to wall stress only control and wall stress plus transpiration velocity control. Furthermore, the region in which the improved predictions occur is limited to approximately the first three grid cells adjacent to the wall.

The results of this simulation show that the prediction of velocity fluctuation intensities can be improved by the addition of a wall-normal velocity approximate boundary condition. But, the fact that the mean velocity profile is not as well predicted when the velocity fluctuations are targeted through the objective function, suggests that the objectives of getting the correct mean velocity profile and the correct rms velocities may be competing objectives.

3.3. Validating the gradient of the objective function

The fact that there was not more improvement in the prediction of the objective profiles with the addition of the transpiration velocity control might suggest that the approximate gradient of the objective function is inaccurate. To validate the gradient computation,

finite difference approximations to the gradient were calculated. This is relatively simple to do. Given a control vector ϕ and a velocity field u, choose a small value of ϵ and perturb the control vector at one point by the amount ϵ (e.g. add ϵ to τ_{12}^w at one point on the lower wall) to obtain a new control vector $\phi + \epsilon \tilde{\phi}$. Now advance the velocity field one time step and explicitly calculate the value of the objective function (2.3), that is, calculate $\mathcal{J}(\phi + \epsilon \tilde{\phi})$. The approximate gradient in the direction $\tilde{\phi}$ is then:

$$\frac{D\mathcal{J}}{D\phi}\tilde{\phi} \approx \frac{\mathcal{J}(\phi + \epsilon\tilde{\phi}) - \mathcal{J}(\phi)}{\epsilon}$$
(3.1)

By comparing the approximation (3.1) to a centered difference approximation, it was found that $\epsilon = 10^{-3}$ produces good approximations to the gradient. By successively perturbing the control vector ϕ at every point it is possible to approximate the entire gradient $D\mathcal{J}/D\phi$. This finite difference gradient approximation can then be compared to the gradient approximated by the adjoint problem described above.

In the case when only wall stress boundary condition controls are used (as in Nicoud et al. (2000)), it was found that the correlation between the two gradient approximations was generally in excess of 90%. When the transpiration velocity control is considered in addition to the wall stress controls, as in the present work, it was found that the correlation between the two gradient approximations was generally in excess of 80%, but in some cases was lower. Thus we are led to believe that the adjoint problem defined above may be yielding satisfactory approximations to the gradient of the objective function, but further work is necessary to determine if the gradient approximation can be improved.

3.4. Is there a simple, linear, general model?

In Nicoud et al. (2000) the data from the sub-optimally controlled simulation at $Re_{\tau}=4000$ in which the wall stresses were used as control was used to derive a simple, linear model to predict the wall stresses from the local velocity field. In short, linear regression was used to find the localized convolution coefficients for the velocity field that best predicted the wall stresses in a least squares sense. This procedure yielded a wall stress model that was inexpensive to compute and accurately reproduced the results of the sub-optimally controlled simulation. Furthermore, this same linear model was able to yield similarly good predictions of the mean velocity profile, for Reynolds numbers ranging from $Re_{\tau}=180$ to $Re_{\tau}=20000$ when the same grid was used as for the sub-optimally controlled simulation. Even when the grid was refined, by the same amount in each direction so that the aspect ratio of the grid remained unchanged, the same linear model continued to produce good results. Further details about the derivation of this wall model can be found in Nicoud et al. (2000).

Unfortunately, as we show here, this simple linear model derived in is not going to be a panacea. Figure 4 shows the mean velocity profiles for several channel flow LES's at $\text{Re}_{\tau} = 4000$ all using the same number of grid points as the simulations discussed above and using the simple linear wall stress model derived in Nicoud *et al.* (2000). In each case some reasonable modification has been made. For instance, a fully conservative fourth order finite difference scheme was used and as shown in the figure, the mean-velocity is under-predicted. To test the effects of the numerics on the efficacy of the wall model, two different things were tried: stretching the grid in the wall-normal direction, and modifying the dynamic procedure as suggested by Cabot & Moin (2000). As Figure 4 shows, the simple linear wall stress model performs worse in every one of these cases than in the original simulation for which it was designed.

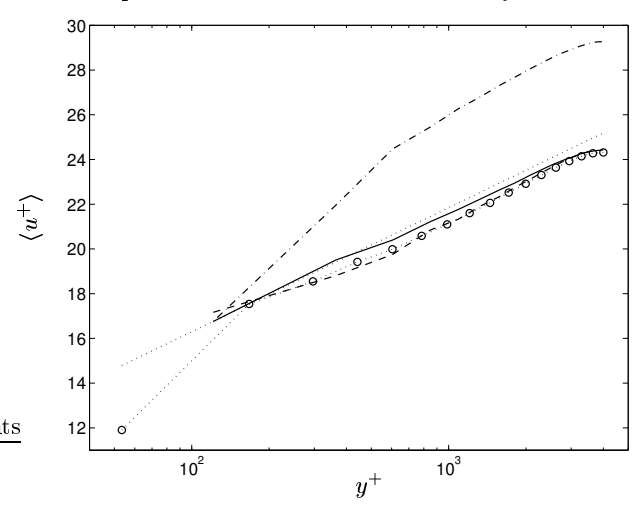


FIGURE 4. Mean velocity profiles using fixed, simple linear model for the wall stresses derived in Nicoud et al. (2000). (········): logarithmic reference profile, $u_{\rm ref}^+=2.41\ln y^++5.2;$ (······): model reproduces mean profile when used in same setting that it was derived; (----): same model with fourth-order finite differences; (-····): same model with modified dynamic procedure as in Cabot & Moin (2000); (·· o ···): same model with stretched wall-normal grid

4. Discussion

It was expected that the addition of the transpiration velocity control would allow the wall model to influence a larger fraction of the flow domain than when using wall stress controls alone. This expectation is is due to two suppositions: 1. a transpiration velocity boundary condition directly effects the entire flow domain through the continuity equation, and 2. the transpiration velocity control should enhance the level resolved turbulence in the near-wall cells leading to less reliance on the inaccurate Smagorinsky SGS model. However, the addition of the transpiration velocity control, while improving matters, does not completely fix everything.

It seems unlikely that approximate boundary condition wall models can do much better than those produced by these sub-optimally controlled simulations (of course, there is still some room to improve the simulations in this work by finding better gradient approximations and exploring other combinations of parameters). There are other culprits at work here, however, for instance the Smagorinsky SGS model is known to be unable to correctly predict the subgrid scale stresses in the logarithmic region at this coarse resolution (Baggett, Jiménez & Kravchenko (1997)). Further efforts to solve the problem of approximate boundary conditions for LES need to be made in tandem with improving the subgrid scale in the anisotropic logarithmic region. The only alternative being to start the LES computation at some plane parallel to the wall beyond which the LES can be trusted. In that case, the boundary conditions for all the velocity components need to be supplied in the interior of the turbulent flow and that problem has been shown to be extremely difficult; see Cabot & Moin (2000) for a review of some of these attempts at finding "off-wall" boundary conditions.

The simple, linear, wall stress model derived in Nicoud *et al.* (2000) was shown to not be robust to changes in the numerical scheme and/or the SGS model. It therefore seems unlikely that any single, explicitly defined simple model is unlikely to work in the variety of flows necessary to make it useful as a predictive tool for LES. Perhaps a more

promising direction is to employ some kind of online optimization or control to force the LES solution near the computational boundaries to match an adaptively computed RANS solution. To this end, B. Mohammadi has proposed a new generalized objective function that would allow the use of more general non-parallel reference velocity profiles by targeting the tangential velocities:

$$\mathcal{J}_{\mathrm{mean},i}(u;\phi) = \int_{-1}^{+1} \left(\delta_{u_t}(y)^2 + \delta_t(y) \right) dy, \tag{4.1}$$

with

$$\delta_{u_t}(y) = \frac{1}{A} \int \int (u_t - u_{t,ref}) \, dx \, dz \tag{4.2}$$

and

$$\delta_t(y) = \frac{1}{A} \int \int ||\vec{t} - \vec{t}_{\text{ref}}|| \, dx \, dz \tag{4.3}$$

where $u_t = \vec{u} \cdot \vec{t}$ is the tangential (to the wall) velocity component. Preliminary computations of the gradient of this objective function, by finite difference approximations, show that the gradients of this new objective function are very different than those of (2.3).

References:

REFERENCES

- BAGGETT, J.S., JIMÉNEZ, J. & KRAVCHENKO, A.G. 1997 Resolution requirements in large-eddy simulations of shear flows. *Annual Research Briefs*, Center for Turbulence Research, 51-66.
- Cabot, W. & Moin, P. 2000 Approximate wall boundary conditions in the large-eddy simulation of high Reynolds number flow. Flow Turb. Combust., 63, 269-291.
- Collis, S.S. & Chang, Y. 1999 On the use of LES with a dynamic subgrid scale model for the optimal control of wall bounded turbulence. In D. Knight and L Sakell, editors. *Recent Advances in DNS and LES*. Kluwer.
- GERMANO, M., PIOMELLI, U., MOIN, P. & CABOT, W. 1991 A dynamic subgrid-scale eddy viscosity model. *Phys. Fluids.*, **3**, 1760-1765.
- Kravchenko, A.G., Moin, P. & Moser, R. 1996 Zonal embedded grids for numerical simulations of wall-bounded turbulent flows. J. Comp. Phys., 127, 412-423.
- NICOUD, F., BAGGETT, J.S., MOIN, P. & CABOT, W. 2000 LES wall modeling based on suboptimal control theory. *To appear in Physics of Fluids*.
- NICOUD, F. & BAGGETT, J.S. 1999 On the use of optimal control theory for deriving wall models for LES. CTR Annual Research Briefs, 329-341.
- PIOMELLI, U., FERZIGER, J., MOIN, P., & KIM, J. 1989 New approximate boundary conditions for large eddy simulations of wall-bounded flows. *Phys. Fluids*, 1, 1061-1068.
- Vainberg, M. 1964 Variational methods for the study of nonlinear operators. Holden Day.